Electromagnetic Characterization of Glass-Fiber-Reinforced Epoxy Composites for Radio-Transparent Enclosures

Ainur Zhetpisbayeva
Department of Radio Engineering, Electronics and Telecommunications, L. N. Gumilyov Eurasian National University, Astana, Kazakhstan
aigulji@mail.ru

Aigul Kulakayeva
Department of Radio Engineering, Electronics and Telecommunications, International Information Technology University, Almaty, Kazakhstan
a.kulakayeva@iitu.edu.kz (corresponding author)

Ainur Zhapanova
Department of Radio Engineering, Electronics, and Telecommunications, S. Seifullin Kazakh Agrotechnical Research University, Astana, Kazakhstan
zhapanovaainur@gmail.com

Kelgenbayev Almas
Electrical Testing Department, Ghalam LLP, Astana, Kazakhstan
a.kelgenbayev@ghalam.kz

Zhumazhanov Berik
Payload and Research & Development Department, Ghalam LLP, Astana, Kazakhstan
b.zhumazhanov@ghalam.kz

Received: 24 March 2026 | Revised: 18 April 2026 | Accepted: 8 May 2026

 DOI: https://doi.org/10.48084/etasr.18909

ABSTRACT

The current study presents the experimental findings on the electromagnetic properties and radio-transparency of glass-fiber reinforced epoxy composites considered for radomes and antenna housings. Three multilayer specimens—L1, L2, and L3—were created through vacuum lamination, differing in internal layer arrangement and having a total thickness from 3 to 4 mm. The impact of the internal structure on the transmission (S21) and reflection (S11) coefficients was studied across 0.5–5.5 GHz using two measurement methods in an anechoic chamber. The first method involved a Vector Network Analyzer (VNA) to capture scattering parameters, while the second used direct signal level measurements with a signal generator and spectrum analyzer. The results showed a frequency-dependent attenuation pattern caused by interference within the multilayer structure. The L1 configuration exhibited notable resonant dips, reaching -5.37 dB at 4.5 GHz. The L3 sample demonstrated relatively stable transmission in the mid-spectrum, but response variability increased at higher frequencies due to larger phase shifts in the thicker layers. The best performance was observed in the L2 design, a symmetric four-layer structure 3 mm thick, showing consistent transmission with amplitude variations below 2 dB across the entire frequency range. Overall, the results suggest that these glass-epoxy composites are suitable for use in radio-transparent antenna components.

Keywords-radio-transparent materials; radome; composite materials; free-space measurement; insertion loss; electromagnetic properties

I. INTRODUCTION

Radio-transparent radomes and housing play an important role in modern radar, satellite navigation, and aerospace systems. Their primary function is to provide mechanical protection for antennas while minimizing electromagnetic interference. Thus, materials used for the manufacture of radomes and radio-transparent housing must combine high mechanical strength, environmental resistance, and excellent electromagnetic transparency. Authors in [1] summarized the results of studies on polymer wave-transparent composites. It was emphasized that, for high-quality transmission of electromagnetic waves in modern communication systems, it is necessary to use polymer matrices with low values of dielectric permittivity (ϵ) and dielectric loss tangent ($\tan\delta$). Authors in [2] discussed the characteristics of glass-fiber-reinforced plastics used in radio-transparent shelters. It was established that E-glass-based reinforcement is of an industrial standard, as it provides an optimal combination of dielectric properties ($\epsilon \approx 4.2$) and mechanical strength.

Nevertheless, challenges remain due to the need to simultaneously ensure ultra-low dielectric permittivity and high thermal stability over a wide frequency range. This is associated with both the high cost and processing complexity of specialized fillers, such as quartz fibers [3, 4], and the intrinsic properties of the materials themselves. For example, aramid yarns exhibit increased hygroscopicity, which deteriorates the stability of dielectric characteristics in humid environments [2, 5]. Additional difficulties arise from contradictions between electrical and structural requirements. Increasing the wall thickness to improve structural strength leads to increased signal losses and phase distortions [6].

To address these issues, hybrid multilayer architectures or modifying additives can be used, allowing precise adjustment of the material impedance. For example, authors in [5, 7] developed hybrid glass-fiber/aramid structures that achieved a transmission coefficient of up to 89.9% over the 1-8.5 GHz range. In [8], it was demonstrated that modifying the binder makes it possible to reduce dielectric losses to as low as 0.03.

However, the accuracy of determining the parameters of such media is often minimized due to the influence of air gaps in measurement cells, while most mathematical models apply only to the X-band (8.2–12.4 GHz) [9]. Authors in [10] explored the narrow range of 5.4–5.9 GHz for meta-surface antennas, using the Nicholson–Ross–Weir algorithm. Thus, there is a need to investigate antenna solutions aimed at a broader range of wireless applications [11].

In addition to limitations in evaluation methods and frequency ranges, significant difficulties arise when attempting to modify the material structure itself in order to improve its functional properties. The integration of Frequency-Selective Surfaces (FSS) to reduce the detectability of Radio-Transparent Shelters (RTS) creates additional challenges [12–14]. Although this approach makes it possible, efforts to reduce the Radar Cross Section (RCS) often result in a narrower operating passband. Materials with ultra-low dielectric permittivity ($\epsilon \approx 1.2$) for 5G systems were investigated in [15], as well as the use of hollow microspheres [16], demonstrating the potential to search for new compositions; however, their application in monolithic load-bearing structures is complicated by the difficulty of scaling. The use of nanoparticles or carbon-based additives [17–20] is primarily focused on electromagnetic shielding and absorption, rendering these methods insufficiently effective for tasks aimed at ensuring maximum radio transparency.

Thus, a study should be conducted on the experimental assessment of the influence of the internal architecture of monolithic glass-fiber-reinforced plastic, in particular, the sequence of alternating glass mat and glass fabric layers, on the stability of the transmission coefficient (S21) and the minimization of interference minima in the demanded frequency range of 0.5-5.5 GHz. This work analyzes the influence of the layer stacking sequence in L1-L3 samples on the interference-related features of electromagnetic wave transmission through structures with a thickness of 3-4 mm.

Hence, this study addresses the existing gap in understanding the relationship between the order of layer alternation and the broadband stability of radio transparency. This relationship often remains overlooked in studies focused on narrow frequency ranges or limited to the investigation of material properties.

The scientific novelty of this work lies in the systematic identification of the relationship between the order of alternating layers with different structures, namely glass mat and glass fabric, and the formation of the interference pattern in the broad frequency range of 0.5–5.5 GHz. Unlike traditional approaches concentrated on averaged dielectric parameters, the present work demonstrates for the first time that controlling the architectural symmetry of the stacking sequence makes it possible to optimize the wave phase shift and to minimize insertion losses solely through the geometric arrangement of the layers.

II. MATERIALS AND METHODS

To determine the electromagnetic characteristics of glass-epoxy composites, two independent free-space measurement methods implemented in an anechoic and shielded chamber were used.

The first method involved the use of a Vector Network Analyzer (VNA) and two broadband horn antennas in a specified frequency range. The antennas were arranged along the same line in a quasi-optical configuration to ensure the incidence of a plane electromagnetic wave on the sample under study. A dielectric mast was installed between the antennas to suspend the sample. To reduce parasitic reflections, radio-absorbing material was placed on the chamber floor. First, free-space attenuation was measured without the sample; the obtained S11 and S21 parameters were recorded and subsequently used for calibration and calculations, as shown in Figure 1(a). Measurements were then performed with the sample installed, and, based on the changes in the S11 and S21 parameters, the transmission losses and reflection characteristics were calculated (Figure 1(b)).

The second method utilized a signal generator and a spectrum analyzer, operating in the required frequency range.

First, the signal attenuation in free space was measured without the sample, and these values were stored as reference values (Figure 2(a)). Measurements were then carried out with the sample installed. Based on these measurements, additional losses and reflected power were calculated, characterizing the radio transparency and insertion losses of the material (Figure 2(b)).

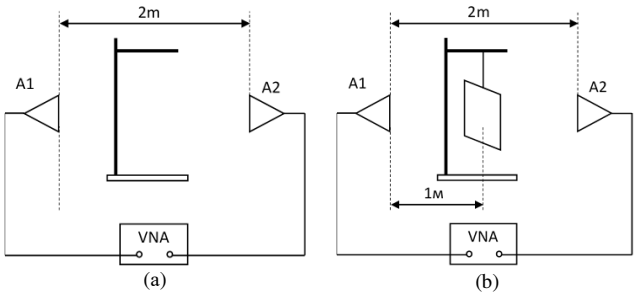

Fig. 1. Measurement scheme of the sample according to Method 1.

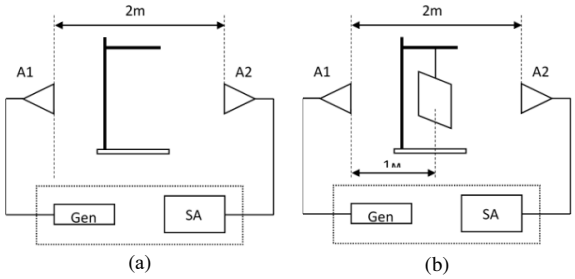

Fig. 2. Measurement scheme of the sample according to Method 2.

The radio transparency and attenuation parameters of the composite material based on glass mat and glass fabric with different layer structures were evaluated using three samples designated as L1, L2, and L3. These samples represented three variants of the internal structure, differing in the order of layer alternation and having a total thickness of 3-4 mm. The sample thicknesses were: L1: 4 mm, L2: 3 mm, and L3: 4 mm. Reinforcement was performed using layers of glass fabric and glass mat, with epoxy resin utilized as the binder material. The choice of materials was based on their dielectric properties: relative permittivity ϵr in the range of 2.5–3.5 and $\tan\delta \leq 0.005$, which satisfy the requirements imposed on low-loss materials for modern radio-transparent structures. All samples had fixed dimensions of 60×60 cm to minimize edge diffraction. Table I presents the detailed layer-by-layer configuration of the composite samples used in the experiment.

TABLE I. LAYER-BY-LAYER STRUCTURE OF THE COMPOSITE SAMPLES UNDER STUDY

Layer number	Sample no. 1 (L1)	Sample no. 2 (L2)	Sample no. 3 (L3)
1	Glass mat	Glass mat	Glass mat
2	Glass fiber	Glass fiber	Glass fiber
3	Glass fiber	Glass fiber	Glass mat
4	Glass fiber	Glass mat	Glass fiber
5	Glass fiber	–	Glass mat
6	Glass mat	–	–

Combinations with alternating glass mat and glass fabric layers of different densities ensure uniform resin distribution and the required mechanical strength. All samples were manufactured using standard vacuum lamination methods to ensure uniform resin distribution and minimal porosity. The tests were carried out in an anechoic chamber with dimensions of 13.3 m in length, 8.8 m in width, and 10.1 m in height. The test frequency range was 0.5–5.5 GHz.

The total distance between the transmitting and receiving horn antennas was 2 m. The sample was placed on a dielectric mast at the center of the measurement line, 1 m from each antenna.

Comparison of data obtained through continuous scanning of the S11 and S21 parameters with the results of signal-level registration at fixed frequencies made it possible to exclude random instrumental errors and confirm the reproducibility of the identified frequency effects. The systematic uncertainty analysis of two independent measurement methods was performed.

For Method 1, the antenna (ETS Lindgren 3117) gain uncertainty was the dominant contribution to the S-parameter measurement uncertainty, at ±1.7 dB (see Appendix 1), while the VNA transmission tracking uncertainty was ±0.061 dB, and the VNA thermal stability contributed ±0.03 dB [21].

For Method 2, employing a Keysight EXG N5171B signal generator and a Keysight N9038A MXE EMI receiver, the additional uncertainty contributors relative to Method 1 include the generator's absolute output level accuracy of ±0.6 dB at 0 dBm gain across 0.5–5.5 GHz, and the receiver amplitude accuracy of ±1.5 dB [22]. Therefore, the instrumental error range is within the appropriate range of ±3 dB.

III. RESULTS

A. *Method 1*

Before beginning the tests, calibration was performed in the frequency range of 0.5-5.5 GHz (Figure 3). Then, the signal level was measured according to Method No. 1 with the test sample installed (Figure 4).

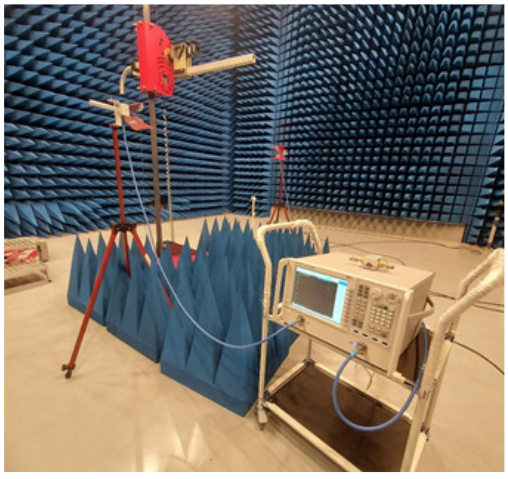

Fig. 3. Calibration of the measurement setup using a VNA.

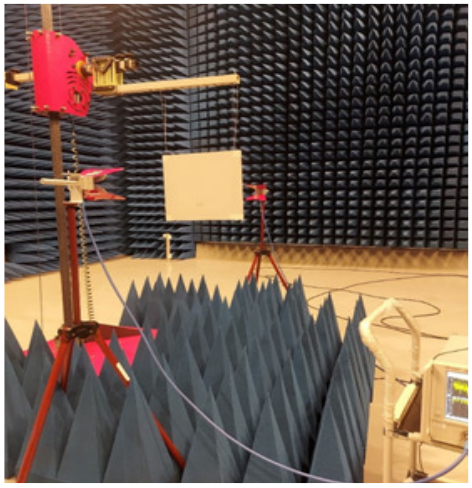

Fig. 4. Measurement scheme of the test sample using a VNA.

After the tests were complete, all data were recorded and processed. Based on these data, a diagram of signal attenuation during transmission through the sample was constructed. The obtained results are presented in Figure 5. In addition, plots of the reflection and transmission coefficients (S11 and S21 parameters) are provided (Figure 6).

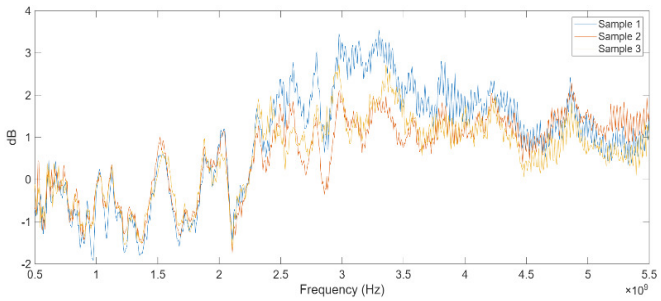

Fig. 5. Frequency dependence of the transmission coefficient (S21 parameter) for the three samples.

The measured transmission coefficient over the 0.5–5.5 GHz range exhibited similar frequency dependence for all samples. In the low-frequency region (up to 2 GHz), minor fluctuations in the transmission level were observed. In the range of 2.5–3.5 GHz, a noticeable increase in insertion losses was recorded, which was particularly pronounced for sample L1. In the 4.5–5.0 GHz region, local transmission maxima and minima were observed for all samples, indicating interference effects due to finite material thickness and reflections within the measurement system. Sample L2 possessed the smoothest and most stable characteristic of the entire frequency range, making the use of a symmetric multilayer structure with a thickness of 3 mm reasonable for radio-transparent applications. Before installing the samples, a reference measurement of the scattering parameters in free space was performed. Figure 6(a) presents the frequency dependences of the reflection coefficient S11, and Figure 6(b) displays the transmission coefficient S21 of the measurement path without a sample in the range of 0.5–5.5 GHz.

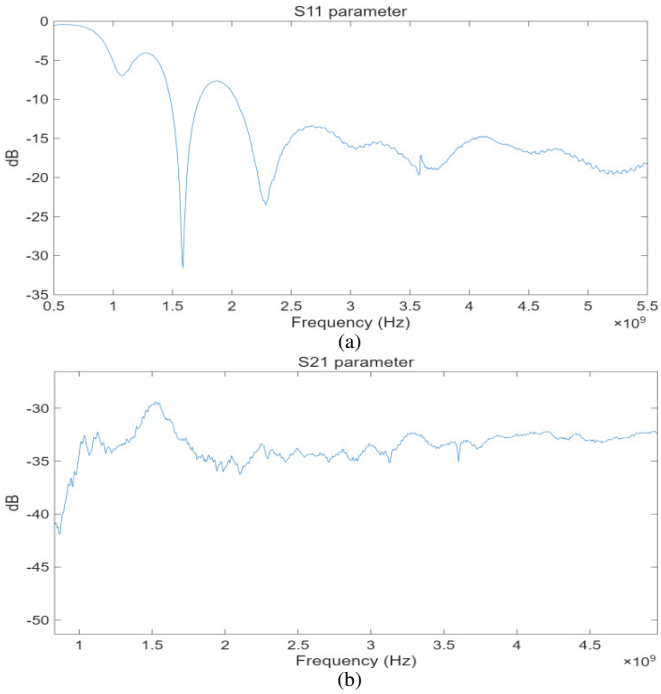

Fig. 6. Signal attenuation in free space of (a) S11 and (b) S21.

The obtained dependences demonstrate a stable transmission coefficient (S21) and satisfactory matching of the measurement system, with S11 being below -10 dB, which is sufficient for a preliminary assessment of the material characteristics. The observed signal-level fluctuations are attributed to interference effects and are explained by the specific features of the free-space measurement scheme. These results were used as reference data when calculating the losses of the samples. After free-space calibration, the L1 sample under study was installed. Figure 7 depicts the frequency dependences of the reflection coefficient S11 (a) and transmission coefficient S21 (b) in the frequency range of 0.5–5.5 GHz.

Figure 8 portrays the frequency dependences of the reflection coefficient S11 (a) and transmission coefficient S21 (b) for sample L2, obtained using the free-space method in the range of 0.5-5.5 GHz. The measurements also showed that the reflection coefficient S11 is predominantly below -10 dB, indicating good matching of the multilayer structure with the air medium.

The frequency dependence of the transmission coefficient S21 is characterized by moderate fluctuations within 2-3 dB, most noticeable in the range of 2.5–3.5 GHz. The wave-like shape of this dependence is caused by interference effects resulting from the finite thickness of the sample and reflections at the interfaces between media.

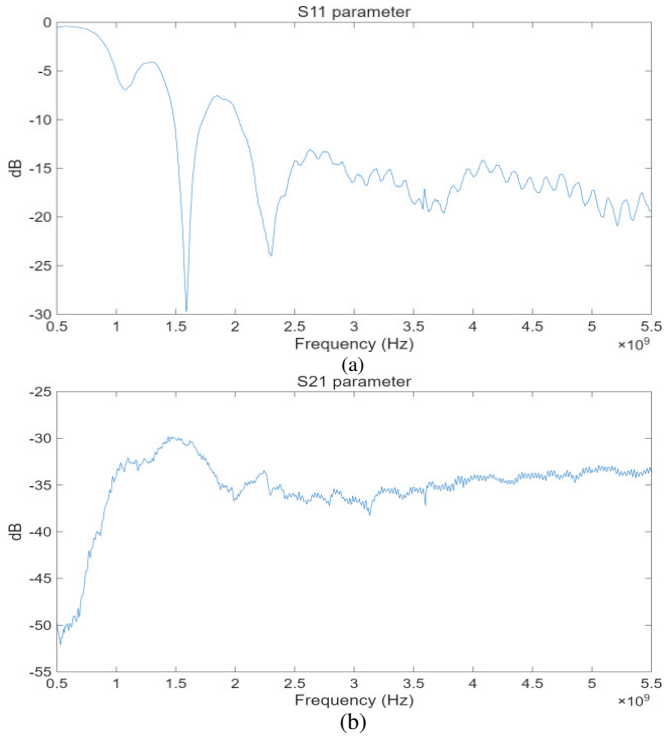

Fig. 7. Sample L1: (a) S11 parameter, (b) S21 parameter.

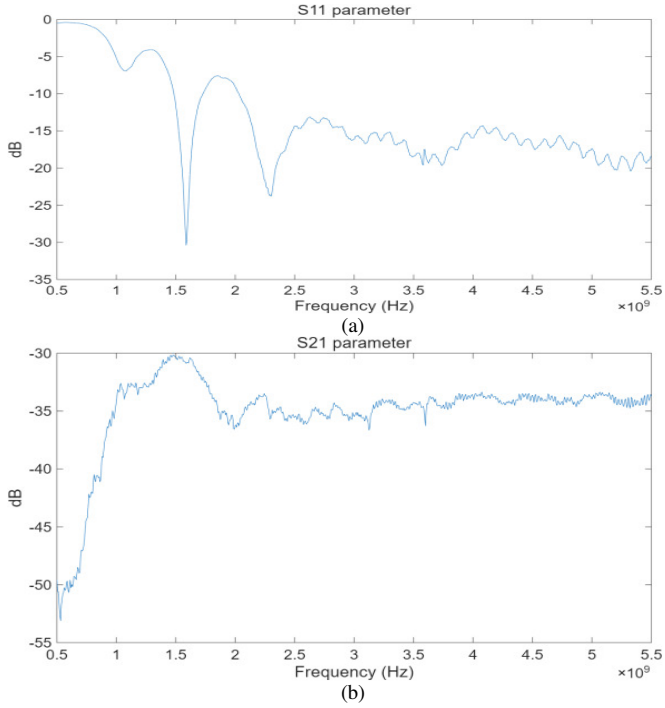

Fig. 8. Sample L2:(a) S11 parameter, (b) S21 parameter.

The frequency dependence of the reflection coefficient S11 indicates effective matching of the structure with the air medium. Across the primary range, the signal level remains below -10 dB. The transmission coefficient S21 exhibits a more gradual variation compared to sample L1. The amplitude of fluctuations does not exceed 2 dB, suggesting a reduction in interference effects.

Therefore, the results confirm that the symmetric four-layer structure with a thickness of 3 mm provides more stable radio-transparent characteristics in the investigated frequency range.

Figure 9 presents the frequency dependences of the reflection coefficient S11 (a) and transmission coefficient S21 (b) for sample L3, measured using the free-space method in the range of 0.5–5.5 GHz.

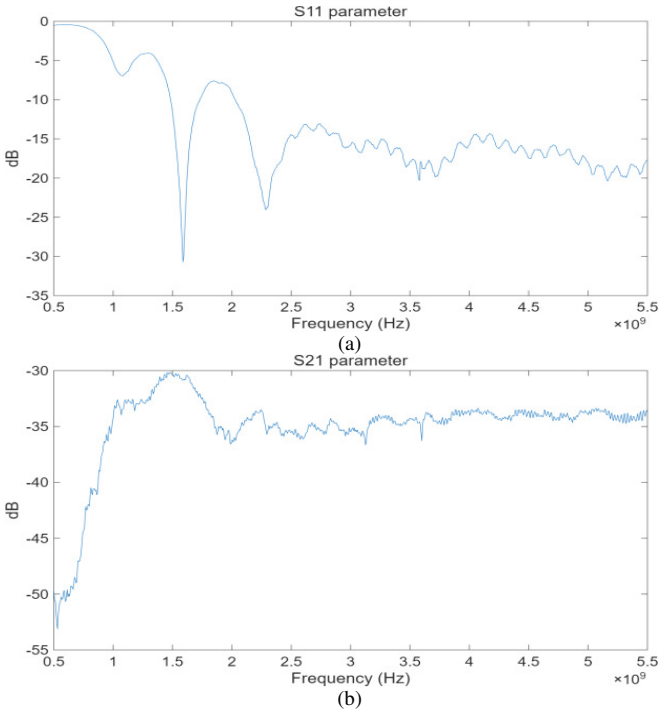

Fig. 9. Sample L3:(a) S11 parameter, (b) S21 parameter.

The reflection coefficient S11 shows good matching with the air medium over most of the investigated frequency range. The dependence of the transmission coefficient S21 on frequency exhibits a pronounced interference pattern, similar to sample L1, but with a slightly lower amplitude of fluctuations.

In the range of 2.5–3.5 GHz, local changes in the transmission level are observed, caused by the phase shift of the wave inside the multilayer structure with a thickness of 4 mm. Overall, sample L3 demonstrates stable radio transparency without a significant increase in dielectric losses.

B. Method 2

Before the tests, calibration was performed in the frequency range of 0.5-5.5 GHz (Figure 10). Then, the signal level was measured according to Method 2 with the test sample installed (Figure 11).

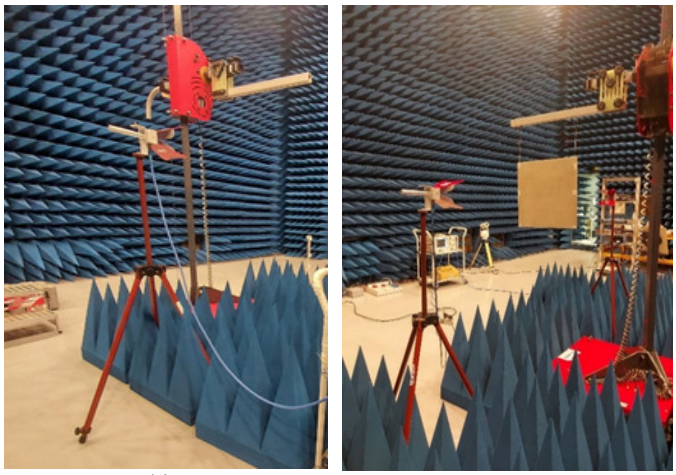

(a) (b)

Fig. 10. Method 2: (a) test setup during calibration, (b) test setup with the test sample.

After the tests, all data were recorded and analyzed, as shown in Table II and Figure 11.

TABLE II. ATTENUATION PARAMETERS

F, MHz	RX CAL_ AVG	RX MEA S N1	RX MEA S N2	RX MEA S N3	L1	L2	L3
1000	-75.18	-77.00	-77.20	-77.93	-1.82	-2.02	-2.75
1500	-71.14	-74.90	-74.04	-73.76	-3.76	-2.90	-2.62
2000	-73.80	-74.50	-74.26	-73.85	-0.70	-0.46	-0.05
2500	-73.36	-74.10	-73.38	-73.56	-0.74	-0.02	-0.20
3000	-74.25	-74.20	-73.68	-73.07	0.05	0.57	1.18
3500	-77.07	-78.4	-77.22	-76.87	-1.33	-0.15	0.20
4000	-76.85	-79.3	-76.88	-78.17	-2.45	-0.03	-1.32
4500	-79.23	-84.6	-82.6	-84.02	-5.37	-3.37	-4.79
5000	-81.47	-80.8	-78.9	-79.32	0.67	2.57	2.15

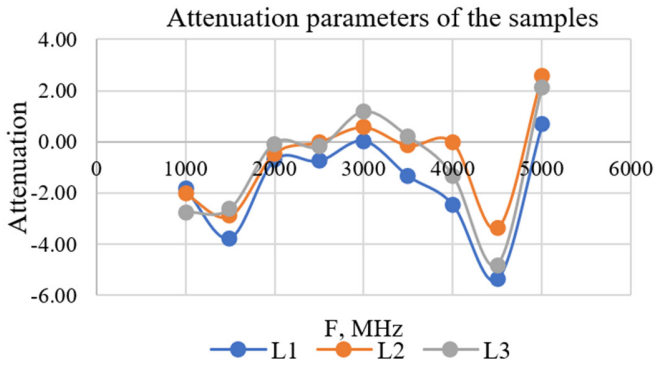

Fig. 11. Attenuation parameters.

The measurement results reveal a pronounced frequency dependence of the attenuation parameters for all investigated samples.

At a frequency of 1 GHz, the insertion losses were -1.82 dB for L1, -2.02 dB for L2, and -2.75 dB for L3. As the frequency increased to 1.5 GHz, signal attenuation increased. The highest value was recorded for L1 (-3.76 dB), while L2 and L3 exhibited values of -2.90 dB and -2.62 dB, respectively.

In the frequency range of 2–2.5 GHz, the attenuation values decreased significantly. At a frequency of 2 GHz, the values ranged from -0.70 to -0.05 dB. At a frequency of 2.5 GHz, the values were -0.74 dB for L1, -0.02 dB for L2, and -0.20 dB for L3.

In the regions of 3 GHz and 5 GHz, the calculated insertion loss values formally exceeded the 0 dB threshold, reaching up to 2.57 dB. This effect is caused by constructive interference and calibration error of the free-space measurement path. These values are interpreted as zones of maximum radio transparency, where the material attenuation is negligibly small and remains within the instrumental error range (±3 dB).

The highest signal attenuation was recorded at 4.5 GHz. The minimum value was registered for L1 (-5.37 dB), while the values for L2 and L3 were -3.37 dB and -4.79 dB, respectively.

At 5 GHz, an increase in the transmission coefficient was observed for all samples. The values were 0.67 dB for L1, 2.57 dB for L2, and 2.15 dB for L3.

Thus, in the 1-5 GHz range, the insertion losses for the investigated samples vary from -5.37 dB to 2.57 dB, confirming the frequency-dependent nature of the attenuation parameter for all configurations of the composite material.

IV. DISCUSSION

The free-space measurement methodology applied in this work fully corresponds to the approaches described in [7, 8, 11]. The obtained data on the average transmission coefficient of glass-fiber-reinforced plastic, approximately 89–90% in the range up to 4 GHz, are almost identical to the results of [7], where a value of 89.01% was recorded for glass-fiber-reinforced plastic based on a similar epoxy resin. This confirms the adequacy of the selected materials and the accuracy of the measurement system calibration. In addition, the general stability of the transmission coefficient observed in this work in the low-frequency region, up to 2 GHz, is consistent with the conclusions of [1] that polymer composites with a dielectric matrix provide minimal phase distortions at long wavelengths.

The first method, using a VNA, provides continuous registration of the S11 and S21 parameters over the entire investigated frequency range. This makes it possible to identify subtle interference features, resonant minima, and local transmission maxima. According to the results obtained using this method, the nature of the frequency fluctuations is mainly caused by wave processes inside the multilayer structure and is not associated with a sharp increase in the dielectric losses of the material. Therefore, it provides high spectral resolution and enables analyzing the distributed effects in the structure.

The second method is based on measuring the absolute level of the received signal at fixed frequencies. Unlike the VNA-based approach, this method records the total energy effect of signal transmission through the material relative to the calibration measurement. The specific method is less sensitive to small-scale interference fluctuations; however, it helps obtain a practical assessment of insertion losses in specific

operating ranges. The results showed comparable trends in attenuation variation for all samples, which confirms the reproducibility of the identified frequency effects.

The comparison of the data obtained by the two methods demonstrates their consistency: the frequency regions with increased attenuation and local transmission maxima coincide. This indicates the physical nature of the observed effects rather than errors in the measurement system. The use of two approaches helped increase the reliability of the obtained results and exclude the influence of the specific features of a single measurement method.

As a result, the differences in the behavior of the samples are determined by their thickness and layer-by-layer architecture, with sample L2 demonstrating the most stable characteristics over a wide frequency range. The application of two independent methods confirmed the suitability of the investigated epoxy glass composites for use in radio-transparent structures. This demonstrates that for highly efficient radio-transparent structures, the determining factor is not only the chemical composition of the materials but also the geometric sequence of the layers, which determines the nature of wave interference inside the structure.

The signal-level fluctuations observed during calibration and measurements, including formal insertion loss values above 0 dB at frequencies of 3 GHz and 5 GHz, are explained by the specific features of the free-space measurement scheme and by standing waves arising due to reflections from tooling elements and interfaces between media. These effects were considered a systematic error, within ±3 dB, and do not affect the overall reliability of the comparative analysis of the samples.

The present study proves that, for developing highly efficient radio-transparent structures, the use of symmetric structures with minimum thickness, as in sample L2, is preferable, since they ensure the most uniform signal transmission and minimize frequency selectivity in the target range from 0.5 to 5.5 GHz.

V. CONCLUSIONS

The most stable radio-transparent characteristics of sample L2 are determined not only by its thickness of 3 mm but also by its symmetric four-layer architecture. This configuration minimizes internal reflections and ensures that the amplitude of fluctuations in the transmission coefficient S21 does not exceed 2 dB, indicating a significant reduction in interference effects compared with the other samples.

The less stable behavior of L3 at high frequencies is directly associated with its increased thickness of 4 mm. In the range of 2.5-3.5 GHz, local changes in the transmission level are observed, caused by the phase shift of the wave inside the multilayer structure, which emphasizes the crucial role of geometric parameters in the design of radio-transparent shelters.

The most pronounced resonant dips observed for sample L1, down to -5.37 dB at a frequency of 4.5 GHz, confirm that the alternation of glass mat and glass fabric layers with different densities creates conditions for intense constructive and destructive interference. This indicates that attenuation in the material is predominantly wave-related in nature and is not associated with dielectric losses of the epoxy resin itself.

A comparison of the results showed that the regions of increased attenuation and transmission maxima fully coincide for both independent methods. This excludes the possibility of interpreting the dips as random instrumental errors and confirms their physical nature.

DECLARATION OF COMPETING INTERESTS

The authors declare that they have no competing interests.

ACKNOWLEDGMENT

This research was funded by the Science Committee of the Ministry of Science and Higher Education, Research Identification Registration Number (IRN) BR27198365 - Development of a short-wave infrared optoelectronic system in the context of the development of remote sensing space systems in Kazakhstan.

DATA AVAILABILITY

The data used and analyzed during this study are available from the corresponding author upon reasonable request.

AI USE AND DECLARATION OF GENERATIVE AI USE

During the preparation of this manuscript, the authors used ChatGPT for translation assistance and language improvement. After using this tool, the authors reviewed and edited the content as needed and took full responsibility for the content of the publication.

REFERENCES

[1] L. Tang, J. Zhang, Y. Tang, J. Kong, T. Liu, and J. Gu, "Polymer matrix wave-transparent composites: A review," *Journal of Materials Science & Technology*, vol. 75, pp. 225–251, Jun. 2021, https://doi.org/10.1016/j.jmst.2020.09.017.

[2] H. Mankodi and S. Parmar, "FRP radome: A short review," *Journal of Aerospace Sciences and Technologies*, pp. 96–103, Jul. 2023, https://doi.org/10.61653/joast.v75i1.2023.7.

[3] I. Haider, I. H. Gul, M. I. Faraz, S. Aziz, S. H. I. Jaffery, M. A. Khan, and D. W. Jung, "Investigation of dielectric, mechanical, and thermal properties of epoxy composites embedded with quartz fibers," *Polymers*, vol. 15, no. 20, Oct. 2023, Art. no. 4133, https://doi.org/10.3390/polym15204133.

[4] L. Zhou, Z. Liu, L. Tang, and Y. Pei, "Design and characterization for a high-temperature dual-band radome wall structure for airborne applications," *Materials and Design*, vol. 114, pp. 264–270, Jan. 2017, https://doi.org/10.1016/j.matdes.2016.11.067.

[5] I. Choi, J. G. Kim, I. S. Seo, and D. G. Lee, "Design of the hybrid composite face with electromagnetic wave transmission characteristics of low-observable radomes," *Composite Structures*, vol. 94, no. 11, pp. 3394–3400, Nov. 2012, https://doi.org/10.1016/j.compstruct.2012.05.017.

[6] G. Pulvirenti, P. D. Tromboni, M. Marchetti, A. Delogu, A. Maccapani, and R. Aricò, "Surveillance system airborne composite radome design," *Kimerius*, 2005. Available: https://www.kimerius.com/app/download/5784678861/Surveillance+system+airbone+composite+radome+design.pdf.

[7] A. Yermakhanova, A. Kenzhegulov, M. Meiirbekov, A. Samsonenko, and B. Baiserikov, "Study of radio transparency and dielectric permittivity of glass- and aramid epoxy composites," *Eurasian Physical*

Technical Journal, vol. 20, no. 2(44), pp. 70–78, Apr. 2023, https://doi.org/10.31489/2023No2/70-78.

[8] A. Yermakhanova, A. Kenzhegulov, B. Baiserikov, M. Meiirbekov, and N. Boguspayev, "Comparative studies of radio transparency and dielectric characteristics of polymer composites," *Journal of Metals, Materials and Minerals*, vol. 34, no. 3, Sep. 2024, Art. no. 1836, https://doi.org/10.55713/jmmm.v34i3.1836.

[9] M. C. Ho and T. H. Le, "Accurate estimation without calibration of the complex relative permittivity of multilayer dielectric material based on the finite integration technique," *Engineering, Technology & Applied Science Research*, vol. 13, no. 3, pp. 10664–10669, Jun. 2023, https://doi.org/10.48084/etasr.5665.

[10] A. S. Ali and I. Ahmed, "Electrical characterization of glass fiber reinforced polymer composites for future metasurface antenna applications," *Materials Research Express*, vol. 8, no. 6, Mar. 2021, Art. no. 065201, https://doi.org/10.1088/2053-1591/ac02fe.

[11] B. Karibayev, N. Meirambekuly, T. Namazbayev, B. Kozhakhmetova, K. Chizhimbayeva, and A. Kulakayeva, "The possibilities of using fractal antennas in modern wireless communication technologies," *in 2023 IEEE International Conference on Smart Information Systems and Technologies*, May 2023, pp. 184–188, https://doi.org/10.1109/SIST58284.2023.10223571.

[12] P. C. Kim, I. S. Seo, and G. H. Kim, "Low-observable radomes composed of composite sandwich constructions and frequency selective surfaces," *Composites Science and Technology*, vol. 68, no. 9, pp. 2163–2170, Jul. 2008, https://doi.org/10.1016/j.compscitech.2008.03.016.

[13] Z. Xing, F. Yang, J. Yang, and X. Zhu, "Low-RCS Ka-band receiving and transmitting satellite communication antennas co-designed with high-performance absorbent frequency-selective radomes," *Journal of Electromagnetic Waves and Applications*, vol. 37, no. 2, pp. 190–206, Jan. 2023, https://doi.org/10.1080/09205071.2022.2118086.

[14] J. Yuan, X. Kong, Q. Wang, and C. Wu, "Intelligent radome design using multilayer metamaterial structures to realize energy isolation and asymmetric propagation of electromagnetic wave," *arXiv*, Mar. 2020, https://doi.org/10.48550/arXiv.2003.02594.

[15] M. Nelo, H. Liimatainen, M. Väätäjä, J. Ukkola, J. Juuti, and H. Jantunen, "Solid air—Low temperature manufacturing of ultra-low permittivity composite materials for future telecommunication systems," *Frontiers in Materials*, vol. 6, May 2019, Art. no. 94, https://doi.org/10.3389/fmats.2019.00094.

[16] X. Zhou, X. Liu, Z. Cui, J. Gu, S. Lin, and Q. Zhuang, "Design and development of HMS@ZIF-8/fluorinated polybenzoxazole composite films with excellent low-k performance, mechanical properties and thermal stability," *Journal of Materials Chemistry C*, vol. 8, no. 22, pp. 7476–7484, Jun. 2020, https://doi.org/10.1039/D0TC00124D.

[17] N. Yesmin and V. Chalivendra, "Electromagnetic shielding effectiveness of glass fiber/epoxy laminated composites with multi-scale reinforcements," *Journal of Composites Science*, vol. 5, no. 8, Aug. 2021, Art. no. 204, https://doi.org/10.3390/jcs5080204.

[18] T. Merizgui, B. Gaoui, T. A. Sebaey, and V. A. Prakash, "Electromagnetic shielding behavior of epoxy multi-hybrid composites comprises of E-glass fiber, Ag nanoparticle, and Ni nanosheet: A novel approach," *Polymer Composites*, vol. 42, no. 5, pp. 2484–2491, Mar. 2021, https://doi.org/10.1002/pc.25993.

[19] P. C. Kim, "Composite sandwich constructions for absorbing the electromagnetic waves," *Composite Structures*, vol. 87, no. 2, pp. 161–167, Jan. 2009, https://doi.org/10.1016/j.compstruct.2008.05.015.

[20] F. B. Gümüş, "Impact of boron-based powder doping on the microwave absorption characteristics of aramid/fiber-glass hybrid composites," *Dokuz Eylül Üniversitesi Mühendislik Fakültesi Fen ve Mühendislik Dergisi*, vol. 28, no. 82, pp. 50–56, Jan. 2026, https://doi.org/10.21205/deufmd.2026288207.

[21] Keysight 2-Port and 4-Port PNA-L Network Analyzer, Keysight Technologies, 2025. [Online]. Available: https://www.keysight.com/zz/en/assets/9018-04407/technical-specifications/9018-04407.pdf.

[22] Keysight X-Series MXE EMI Receiver, Keysight Technologies, 2023. [Online]. Available: https://www.keysight.com/zz/en/assets/9018-04935/technical-specifications/9018-04935.pdf.